K-shell ionization of elements $_{15}$P to $_{28}$Ni for 0.4 to 3.8 MeV/amu $^{10}_{5}$B-ion bombardment

G. Monigold,* F. D. McDaniel, J. L. Duggan, R. Rice, A. Toten, and R. Mehta
Department of Physics, North Texas State University, Denton, Texas 76203

P. D. Miller
Oak Ridge National Laboratory, Oak Ridge, Tennessee
(Received 27 December 1977)

K-shell x-ray production cross sections, $K\beta/K\alpha$ x-ray intensity ratios and $K\alpha$ and $K\beta$ x-ray energy shifts have been determined for thin solid targets of $_{15}$P, $_{19}$K, $_{20}$Ca, $_{21}$Sc, $_{22}$Ti, $_{23}$V, $_{25}$Mn, $_{26}$Fe, $_{27}$Co, and $_{28}$Ni for 4–38-MeV $^{10}_{5}$B ion bombardment. Comparisons of the cross sections were made to direct Coulomb ionization and electron-capture theories by means of fluorescence yields corrected for multiple-ionization effects. The dominant contribution to K-vacancy production for these projectile-target combinations is believed to be direct ionization. Electron capture is expected to be important only for the lighter target elements and then primarily at the higher velocities. The direct-ionization theories employed were the binary-encounter approximation and the plane-wave Born approximation (PWBA) both of which overestimated the experimental data especially at the lower incident ion velocities. The PWBA was modified for increased target-electron binding, Coulomb deflection of the incident ion, polarization of the target-electron wave functions due to the passage of the incident ion, and relativistic target-electron velocities. The experimental data were found to agree quite well with the sum of the theoretical predictions of the modified PWBA and electron capture.

I. INTRODUCTION

In recent years, a great deal of research has involved inner-shell ionization produced through ion impact. The two primary types of inner-shell-vacancy production mechanisms that have evolved are (i) Coulomb ionization[1] caused by the interaction between the incident ion and the ejected electron and (ii) electron promotion[2,3] due to the formation of quasimolecular orbitals during the collision. These very different excitation mechanisms are believed to be appropriate only for certain ranges[4] of the parameters Z_1/Z_2 and v_1/v_e, where Z_1 and Z_2 are the atomic numbers of the incident ion and target atom, respectively, and v_1 and v_e are the ion velocity and target-electron velocity, respectively. For $Z_1/Z_2 \ll 1$ or $v_1/v_e \gtrsim 1$, direct Coulomb ionization is the dominant mechanism, while for $Z_1/Z_2 \sim 1$ and $v_1/v_e \ll 1$, electron promotion is expected to be the principal excitation mechanism. For heavier incident ions at intermediate velocities such that $Z_1/Z_2 < 1$ and $v_1/v_e < 1$, K-electron transfer to bound states of the projectile has been found to be very important in target K-vacancy production.[5-9] For heavier projectiles at higher velocities such that $Z_1/Z_2 \lesssim 1$ and $v_1/v_e \gtrsim 1$, experiments have indicated that charge transfer is not as important in K-vacancy production, and direct Coulomb ionization again dominates.[10]

Both classical and quantum-mechanical approaches have been employed to calculate direct Coulomb ionization. The binary-encounter approximation (BEA) developed by Garcia *et al.*,[11] the semiclassical approximation (SCA) developed by Bang and Hansteen[12] and Hansteen and Mosebekk,[13] and the plane-wave Born approximation (PWBA) developed by Merzbacher and co-workers[14,15] have all been reasonably successful for light-ion ($Z \leq 4$) bombardment of heavier target atoms at ion energies greater than a few MeV. For heavier incident ions at lower velocities the theoretical calculations overestimate the experimental cross sections owing to Coulomb deflection of the incident ion by the target nucleus and to increased binding of the target electron due to penetration of the K shell by the projectile. The BEA has been modified by Thomas and Garcia[16] for Coulomb deflection and by Hansen[17] for increased binding, Coulomb deflection, and relativistic effects. The PWBA has been modified by Basbas *et al.*[18] for Coulomb deflection and increased target-electron binding energy. These modifications to the earlier theoretical approaches are necessary because of simplifying assumptions made concerning the interaction between the incident ion and the target electron. Basbas et al.[19-21] have recently shown that further modifications to the PWBA are necessary owing to polarization of the target-electron wave function by high-velocity ions. The PWBA modified for increased binding, Coulomb deflection, polarization, and relativistic effects has provided very good predictions of experimental x-ray-production cross sections for $Z_1/Z_2 \ll 1$.[22-28]

K-vacancy production in heavy-ion collisions

has been explained by Meyerhof and co-workers[29-36] in terms of a number of basic molecular-orbital (MO) excitation processes that are based upon simplified MO correlation diagrams from the well-known work of Barat and Lichten.[3] According to Meyerhof and Anholt[32] the four basic processes that govern K-vacancy production in heavy-ion collisions are (i) excitation of $1s\sigma$ vacancies, primarily by ionization[30,35]; (ii) excitation of $2p\sigma$ vacancies by two-step processes such as $3p\pi$-$2p\pi$ radial coupling and $2p\pi$-$2p\sigma$ rotational coupling,[34] as discussed by Fastrup,[37] and by ionization[30]; (iii) sharing of $2p\sigma$ vacancies between higher-Z and lower-Z collision partners[29-34]; and (iv) excitation of $3d\sigma$ vacancies through a variety of possible couplings and giving rise to KL level matching[36] as discussed by Barat and Lichten.[3]

While both Coulomb ionization and molecular-orbital excitation approaches to inner-shell-vacancy production have been employed quite successfully in their respective regimes, considerable disagreements between experiments and theories still exist in intermediate regions of Z_1/Z_2 and v_1/v_e.

The aim of the present work is to measure x-ray-production cross sections in a region of the parameters Z_1/Z_2 and v_1/v_e, where Coulomb ionization should be the dominant excitation mechanism. In particular, measurements have been made of K-shell x-ray-production cross sections, x-ray energy shifts, and $K\beta/K\alpha$ x-ray-intensity ratios for 4- to 38-MeV $^{10}_{5}$B ion bombardment of thin solid targets of $_{15}$P, $_{19}$K, $_{20}$Ca, $_{21}$Sc, $_{22}$Ti, $_{23}$V, $_{25}$Mn, $_{26}$Fe, $_{27}$Co, and $_{28}$Ni. For the present work the ranges of the parameters Z_1/Z_2 and v_1/v_e lie between $0.18 \leq Z_1/Z_2 \leq 0.33$ and $0.14 \leq v_1/v_e \leq 0.84$. The experimental x-ray-production cross sections are compared to theoretical predictions obtained from the BEA, the PWBA, the PWBA with binding-energy (B) and Coulomb-deflection (C) modifications (PWBA-BC), and the PWBA-BC with a modification for polarization (P) and an approximate correction for relativistic (R) effects (PWBA-BCPR). In addition to the direct-ionization mechanisms, the contribution to the cross sections from electron capture is included. Preliminary portions of this work have been presented earlier.[38]

II. EXPERIMENTAL PROCEDURES

The $^{10}_{5}$B ions of energy 4–38 MeV were obtained from the Tandem Van de Graaff accelerator at ORNL. The incident charge states of the ions were 2+, 3+, 4+, or 5+ and were selected by the energy of interest. The experimental procedure has been discussed earlier[26] and will only be briefly presented here. The incident ion beam was collimated by two Ta apertures 1 mm in diameter separated by 40 cm and located approximately 50 cm in front of the scattering chamber and by a 3-mm-diam carbon aperture at the chamber entrance. Thin transmission targets, which were vacuum deposited on 10–30-μg/cm^2 carbon backings, were mounted at 45° with respect to the incident-beam direction. The targets used in this experiment and their respective *in-beam* thicknesses are listed in Table I. An Ortec Si(Li) detector with a full width at half maximum resolution of 180 eV at 5.9 keV was positioned inside the target chamber approximately 5 cm from the target and at 90° to the incident-beam direction. Initially, data were collected for target species $_{20}$Ca through $_{28}$Ni with a 0.10-mm Mylar attenuator installed between the target position and the Be window of the detector to reduce possible contributions to the counting rate from the L-shell radiations of the heavier-target elements. The 0.10-mm Mylar attenuator was then replaced by a 0.013-mm Mylar attenuator and data were collected for the elements $_{15}$P, and $_{19}$K through $_{23}$V.

The absolute efficiency of the Si(Li) detector was measured using standard calibrated radioactive sources of ^{54}Mn, ^{57}Co, and ^{241}Am for the data collected when the 0.10-mm Mylar attenuator was installed. The procedures for measuring the efficiencies are outlined elsewhere.[39,40] The sources were mounted at target locations in the chamber to simulate the actual experimental geometry and include the fractional solid angle of the Si(Li) detector. For the data collected using the 0.013-mm Mylar attenuator, the absolute-efficiency measurements were repeated for energies above 3.3 keV. At x-ray energies below 3.3 keV, the efficiency was calculated using the method des-

TABLE I. Target thickness.[a]

Element	Z_2	μg/cm^2
P (Zn_3P_2)	15	5.2
K (KBr)	19	11.0
Ca (CaF_2)	20	18.2
Sc	21	73.7
Ti	22	43.2
V	23	21.4
Mn	25	84.5
Fe	26	23.0
Co	27	17.0
Ni	28	79.4

[a] Measured with the target positioned in-beam at an angle of 45° with respect to the incident-beam direction.

cribed by Gallagher and Cipolla.[40] The detector solid angle was included by comparing the calculated efficiencies at the energies where the intrinsic efficiency of the x-ray detector was 100% to the measured efficiency of the 13.9 keV ^{237}Np $L\alpha$ x-ray line from the ^{241}Am decay. The resulting efficiency curves obtained for the 0.10- and 0.013-mm Mylar absorbers are presented in Fig. 1.

Si surface-barrier detectors were mounted in the scattering chamber at 30° and 45° to the incident-beam direction to detect the $^{10}_{5}$B ions elastically scattered from the target elements. The solid angles of the particle detectors were measured with a calibrated radioactive ^{244}Cm source and found to be 8.09×10^{-4} sr for the 30° detector and 7.95×10^{-4} sr for the 45° detector. The absolute magnitude of the experimental cross sections were then calculated by normalizing the x-ray yield to the Rutherford differential cross section of the scattered $^{10}_{5}$B ions. In anticipation of non-Rutherford contributions to the elastic-scattering process from the target elements at the higher incident-ion energies, a 100 μg/cm^2 self-supporting Au foil was installed 20 cm behind the scattering chamber at an angle 45° to the incident-beam direction. A surface-barrier detector was mounted at 90° to the beam direction with a 4.8-mm-diam aperture approximately 10 cm from the Au target. It was expected that the $^{10}_{5}$B ions elastically scattered from the Au would be Rutherford in nature over the entire energy range.[41,42] This measurement allowed the determination of the ratio of the scattered-ion yield from the Au to the scattered-ion yield from the target material at the lower incident-ion energies. Using this ratio, absolute normalization to the Rutherford differential cross section of Au could be used over the entire energy range.

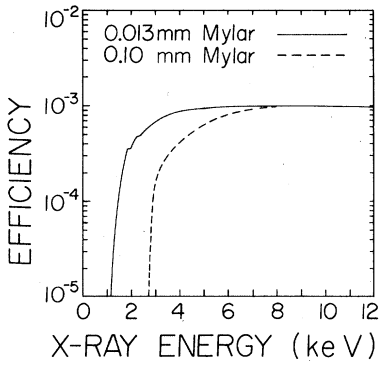

FIG. 1. Absolute lithium-drifted silicon x-ray-detector efficiencies for 0.10-mm-Mylar and for 0.013-mm-Mylar attenuators. The curves include both the intrinsic detector efficiency and the detector solid angle ($\sim 10^{-3}$ sr). The curve for the 0.013-mm-Mylar attenuator is calculated by the method described in Ref. 40 for x-ray energies below 3.3 keV and is measured for x-ray energies above 3.3 keV.

The x-ray and charged-particle spectra were both input to 1024 channels of a Tennecomp Pace System analog-to-digital converter (ADC) which was interfaced with a PDP 11/45 computer. The computer had light-pen spectra-reduction capabilities. The counting rates were low enough that the detector dead time remained essentially zero. The dead time of the ADC, which was generally less than 10%, was used to determine the dead-time correction to the measured yields.

III. DATA ANALYSIS

X-ray production cross sections were determined from the expression

$$\sigma_{Kx}(E)=\left(\frac{Y_{K\alpha}}{\epsilon_{K\alpha}}+\frac{Y_{K\beta}}{\epsilon_{K\beta}}\right)\sigma_R(E,\theta)\,\frac{d\Omega_R(\theta)}{Y_R(E,\theta)}\,\tau_{\mathrm{DT}}\,T\ , \tag{1}$$

where $Y_{K\alpha}$ and $Y_{K\beta}$ are the $K\alpha$ and $K\beta$ x-ray yields, respectively; $\epsilon_{K\alpha}$ and $\epsilon_{K\beta}$ are the Si(Li) detector efficiencies at the observed $K\alpha$ and $K\beta$ x-ray energies; $\sigma_R(E,\theta)$ is the Rutherford differential cross section at incident-ion energy E and scattering angle θ; $d\Omega_R(\theta)$ is the particle-detector solid angle; $Y_R(E,\theta)$ is the yield of scattered $^{10}_{5}$B ions at angle θ; τ_{DT} is the electronic dead-time correction for both the x-ray and scattered-ion yields; and T is a correction factor for energy lost in the thin-target foil.

The factor T, which has been described by Laubert *et al.*,[43] is an approximate correction to both the x-ray and scattered-ion yields for energy loss of the ions in passing through the targets of finite thickness. For the 84-μg/cm^2-thick Mn target (see Table I), the combined correction to the x-ray and scattered-ion yields was ~1% at the highest ion energy and ~17% at the lowest ion energy.

Target x-ray self-absorption was determined for the lowest x-ray energies and was found to be less than 0.5%. Equation (1) assumes isotropy of K x-ray emission, which has been verified by a number of workers.[44] Recoil effects[45-48] in x-ray cross-section measurements are expected to be negligible until $Z_1 \gtrsim Z_2$ and then only for small values of the direct-ionization cross section.[48]

X-ray energy shifts and $K\beta/K\alpha$ ratios have also been determined. Absolute energy shifts were obtained by comparison of the observed target x-ray-energy centroid resulting from $^{10}_{5}$B-ion bombardment to that expected from an energy calibration determined with a number of radioactive sources and checked at each ion energy. For the lower-Z

targets, the resolution afforded by the x-ray spectrometer system did not allow complete separation of the $K\alpha$ and $K\beta$ x rays. For these lower Z elements, the $K\alpha$ and $K\beta$ x-ray peak centroids and yields were determined with a computer peak-fitting routine SAMPO.[49]

IV. THEORETICAL CALCULATIONS

The BEA calculations are made according to prescriptions given by McGuire and Richard.[50] The PWBA calculations are made after procedures given by Basbas, Brandt, and Laubert.[18] The K-shell-ionization cross section in the PWBA formalism is given[18] by

$$\sigma_K^{\mathrm{PWBA}} = (\sigma_{0K}/\theta_K)F(\eta_K/\theta_K^2) , \tag{2}$$

where

$$\sigma_{0K} = 8\pi a_0^2 (Z_1/Z_{2K}^2)^2 , \tag{3}$$

$$\theta_K = U_K/Z_{2K}^2 \mathcal{R} , \tag{4}$$

$$\eta_K = v_1^2/(Z_{2K} v_0)^2 , \tag{5}$$

$$Z_{2K} = Z_2 - 0.3 . \tag{6}$$

In the previous expressions, θ_K is the reduced binding energy, η_K is the reduced particle-velocity parameter, Z_1 and Z_2 are the nuclear charges of the projectile and target, respectively, a_0 is the Bohr radius, U_K is the K-shell binding energy, $\mathcal{R}$ is the Rydberg constant, v_1 is the projectile velocity, and v_0 is the Bohr velocity. F is a universal function[18] of η_K/θ_K^2 and is equal to $(\theta_K/\eta_K)f_K$, where $f_K(\eta_K, \theta_K)$ is tabulated by Khandelwal, Choi, and Merzbacher.[51]

Basbas *et al.*[18] have introduced modifications to the PWBA for Coulomb deflection of the projectile and increased target-electron binding energy due to the penetration of the K shell by the projectile. The PWBA incorporating these modifications (PWBA-BC) is given by

$$\sigma_K^{\mathrm{PWBA\text{-}BC}} = 9E_{10}(b\epsilon\theta_K\eta_K^{-3/2})(\sigma_{0K}/\epsilon\theta_K)F(\eta_K/\epsilon^2\theta_K^2) , \tag{7}$$

where E_{10} is an exponential integral of order 10, b is a constant for a particular projectile-target combination, and ϵ is the binding-energy modification factor. The first factor in Eq. (7) incorporates the Coulomb-deflection modification. The binding energy θ_K is modified by replacing θ_K by $\epsilon\theta_K$ with $\epsilon \geq 1$. Both binding-energy and Coulomb-deflection effects are expected to reduce the ionization probability, particularly for lower incident-ion velocities.

Basbas *et al.*[21] have further modified the PWBA to include effects attributed to polarization of the target-electron wave function by the high-velocity incident ions. The polarization effect is expected to decrease the target-electron binding energy and result in an increase in the ionization probability. The polarization effect is incorporated in the PWBA by Basbas *et al.*[21] by a further modification of the reduced binding energy θ_K. θ_K is replaced by $\zeta\theta_K$, which includes binding-energy and polarization effects. The PWBA with binding-energy, Coulomb-deflection, and polarization modification (PWBA-BCP) is given by

$$\sigma_K^{\mathrm{PWBA\text{-}BCP}} = 9E_{10}(b\zeta\theta_K\eta_K^{-3/2})(\sigma_{0K}/\zeta\theta_K)F(\eta_K/\zeta^2\theta_K^2). \tag{8}$$

The inclusion of binding-energy and polarization developments to the PWBA produces values of $\epsilon\theta_K$ or $\zeta\theta_K$ outside the range of θ_K tabulated by Khandelwal, Choi, and Merzbacher.[51] In order to reduce uncertainties in the PWBA calculations from extrapolations out of the existing table[51] of $f_K(\eta_K, \theta_K)$ functions, we have numerically integrated the universal functions F used in the calculation of K-shell cross sections. The tabulated results of the numerical integrations for F for values of $0.01 \leq \eta_K/\theta_K^2 \leq 95$ and $0.4 \leq \theta_K \leq 3$ are presented elsewhere.[52]

For ions incident on higher-Z targets at lower ion velocities, relativistic effects are expected to be important.[53,54] Relativistic corrections were incorporated through an approximate method of Hansen.[17] The relativistic correction consists of a multiplicative factor to the BEA cross sections and is expected to increase the theoretical cross sections at lower incident-ion velocities. This correction has been made to the PWBA cross sections in the present work. The PWBA with modifications for increased binding-energy, Coulomb-deflection, polarization, and relativistic effects is labeled PWBA-BCPR.

For heavier projectiles, K-electron transfer to bound states of the projectile can be important to K-vacancy production in the target.[5-9] Theoretical calculation of inner-shell ionization through K-electron capture (EC) by heavy charged particles have been reported by Lapicki and Losonsky.[8] They use the analytical expressions of Nikolaev[55] with screened hydrogenic wave functions in the Oppenheimer[56] and Brinkman-Kramers[57] approximation and include modifications for increased binding and Coulomb-deflection effects in a manner similar to that used by Basbas *et al.*[18] for direct ionization. McDaniel *et al.*[9] have further modified this approach to electron capture by means of a reduced-binding-energy effect. These improved calculations simultaneously demonstrated the validity of this approach to electron capture through the charge-state dependence of the cross

TABLE II. PWBA direct-ionization cross sections with and without modifications for increased binding (B), Coulomb deflection (C), polarization (P), and relative effects (R) for $^{10}_{5}$B-ion bombardment. The contributions of electron capture (EC) weighted by the equilibrium-charge-state fractions of the incident $^{10}_{5}$B ion have been added to the fully modified direct-ionization cross sections. All cross sections are in barns (10^{-24} cm^2). Numbers in parentheses denote powers of ten, e.g., 1.22(5) = 1.22×10^5.

	$_{15}$P		$_{28}$Ni	
	8 MeV	38 MeV	4 MeV	38 MeV
PWBA	1.22(5)	3.89(5)	5.56(1)	1.07(4)
PWBA-B	4.58(4)	3.37(5)	4.95	7.09(3)
PWBA-C	1.21(5)	3.89(5)	4.80(1)	1.07(4)
PWBA-BC	4.54(4)	3.37(5)	4.05	7.05(3)
PWBA-BCP	7.23(4)	4.64(5)	4.08	8.70(3)
PWBA-BCPR	7.26(4)	4.64(5)	4.89	8.85(3)
EC	2.05(4)	1.55(5)	3.77(-2)	5.57(2)
(PWBA-BCPR) + EC	9.31(4)	6.19(5)	4.93	9.41(3)

sections and the applicability of the perturbed stationary-state theory of direct ionization of Basbas *et al.*[18,21] for values of $0.44 \leq Z_1/Z_2 \leq 0.67$.

The PWBA direct-ionization cross sections with and without modifications for increased binding (B), Coulomb-deflection (C), polarization (P), and relativistic effects (R) are given in Table II for two representative incident-ion energies and two representative target atoms. One observes that the modification for Coulomb deflection of the "heavy" $^{10}_{5}$B ion is quite small in comparison to the binding-energy effect. The polarization effect is largest at higher velocities and for larger values of Z_1/Z_2. Relativistic corrections are more important at lower incident-ion velocities for heavier target elements. The contributions to the cross sections of electron capture (EC) weighted by the equilibrium charge-state distributions[58,59] of the $^{10}_{5}$B ion is also given in Table II. Electron capture is found to be quite important for $_{15}$P ($Z_1/Z_2 = 0.33$) while of little importance for $_{28}$Ni ($Z_1/Z_2 = 0.18$) at these ion velocities.

V. RESULTS AND DISCUSSION

The x-ray-production cross sections, $K\beta/K\alpha$ ratios, and x-ray-energy shifts determined in the present investigation are presented in Table III. The sources of uncertainties in the x-ray-production cross sections are presented in Table IV and are 7%–12% except for $_{15}$P and $_{19}$K, where the uncertainties increase to 14%–20%. The uncertainties in the $K\beta/K\alpha$ ratios are primarily from statistical uncertainties in the x-ray yields and backgrounds and range from 6%–9%. The uncertainties in the $K\alpha$ and $K\beta$ x-ray-energy shifts are primarily caused by the uncertainty in the location of the x-ray peak centroids and the stability of the Si(Li) spectrometer system. These uncertainties have been estimated to be < 10 eV and < 20 eV, respectively.

In order to compare x-ray-production cross sections determined from experiment with ionization cross sections, the fluorescence yield must be used. The philosophy has been adopted in this paper that the experimental data should not be modified by fluorescence-yield factors but rather will be presented as measured, and that all theoretical ionization cross sections will be converted to x-ray production cross sections for comparisons.

If large amounts of multiple ionization of the target atom are present during the "heavy" ion-atom collision, the fluorescence yields for single-hole ionization ω_0, may not be appropriate.[60] Multiple ionization of the target atom has been shown to cause shifts in the x-ray energies and changes in the x-ray intensities which produces changes in the fluorescence yields. Figure 2 presents measured x-ray-energy shifts in $K\alpha$ and $K\beta$ x-ray transitions for $^{10}_{5}$B-ion bombardment of $_{19}$K and $_{23}$V. One observes that the maximum x-ray energy shifts occur when the ratios of $^{10}_{5}$B-ion velocity (v_1) to the average L-shell electron velocity ($\overline{v}_L$) are close to one. Therefore, the majority of the K x-ray-energy shift may be attributed to the presence of multiple L-shell vacancies at the time of the K-vacancy decay. In order to be able to estimate the changes in fluorescence yields, we have used the scaling procedure of Larkins.[61] Changes in the fluorescence yields have been determined for the defect configuration by scaling the radiative and Auger transition rates given by McGuire[62] by the fraction of the number of $2p$ electrons present in the L shell. Because of the approximations present in this technique and to simplify the calculation, it was assumed that the x-ray-energy shifts come entirely from $2p$ vacancies. Vacancies in the $2s$, $3s$, $3p$, and $3d$ shells have been neglected. The number of $2p$ vacancies were inferred by comparing the measured $K\alpha$ and $K\beta$ x-ray-energy shifts to that expected from Hartree-Fock-Slater calculations.[63] Table V presents ratios of fluorescence yields calculated by the above technique to those calculated for the *no-defect* configuration.

Figure 3 presents a representative sample of cross sections determined in the present work. Experimental x-ray-production cross sections for $_{15}$P, $_{19}$K, $_{23}$V, and $_{28}$Ni are compared to theoretical predictions of the BEA, the PWBA, the

TABLE III. Experimental K-shell x-ray-production cross sections, $K\beta/K\alpha$ x-ray-intensity ratios, and $K\alpha$ and $K\beta$ energy shifts for $^{10}_{5}$B-ion bombardment.

Element	E (MeV)	$\sigma_{Kx} \pm \delta\sigma_{Kx}$ [a] (b)	$K\beta/K\alpha$ [b]	$\Delta E_{K\alpha}$ [c] (eV)	$\Delta E_{K\beta}$ [c] (eV)
$_{15}$P	8	5.52 ± 1.10(3)	0.107		80
	10	9.50 ± 1.90(3)	0.100		81
	12	1.76 ± 0.35(4)	0.081		83
	22	3.43 ± 0.69(4)	0.094		47
	26	4.24 ± 0.85(4)	0.089		53
	30	4.86 ± 0.83(4)	0.094		35
	34	4.50 ± 0.77(4)	0.074		50
	38	4.00 ± 0.70(4)	0.076		34
$_{19}$K	8	9.27 ± 1.39(2)	0.106	35	121
	10	1.67 ± 0.25(3)	0.102	33	117
	12	3.18 ± 0.48(3)	0.102	33	112
	14	4.88 ± 0.73(3)	0.116	34	108
	18	7.94 ± 1.19(3)	0.113	24	90
	22	1.33 ± 0.20(4)	0.114	21	79
	26	1.80 ± 0.27(4)	0.122	23	75
	30	1.96 ± 0.30(4)	0.120	18	63
	34	2.42 ± 0.36(4)	0.123	18	61
	38	2.20 ± 0.33(4)	0.119	15	54
$_{20}$Ca	4	2.55 ± 0.21(1)	0.130	26	95
	6	1.63 ± 0.12(2)	0.135	30	107
	8	4.77 ± 0.36(2)	0.134	38	110
	10	1.23 ± 0.09(3)	0.150	36	118
	12	2.34 ± 0.17(3)	0.149	34	118
	14	3.79 ± 0.28(3)	0.148	31	110
	18	7.30 ± 0.54(3)	0.143	29	94
	22	1.06 ± 0.08(4)	0.125	25	90
	26	1.38 ± 0.10(4)	0.126	23	87
	30	1.50 ± 0.30(4)	0.123	21	75
	34	1.93 ± 0.30(4)	0.142	18	67
	38	2.13 ± 0.17(4)	0.141	19	54
$_{21}$Sc	4	1.85 ± 0.16(1)	0.109	23	81
	6	9.73 ± 0.77(1)	0.136	29	91
	8	3.32 ± 0.26(2)	0.149	31	89
	10	8.59 ± 0.65(2)	0.155	35	109
	12	1.64 ± 0.12(3)	0.146	36	111
	14	2.67 ± 0.19(3)	0.145	32	106
	18	5.56 ± 0.41(3)	0.141	31	100
	22	9.05 ± 0.66(3)	0.150	23	90
	26	1.21 ± 0.09(4)	0.150	23	69
	30	1.43 ± 0.24(4)	0.140	22	71
	34	1.49 ± 0.30(4)	0.147	23	70
	38	1.70 ± 0.30(4)	0.144	18	58
$_{22}$Ti	4	1.41 ± 0.12(1)	0.124	18	73
	6	7.04 ± 0.54(1)	0.133	28	92
	8	2.18 ± 0.16(2)	0.142	32	105
	10	5.52 ± 0.41(2)	0.152	34	108
	12	1.14 ± 0.08(3)	0.145	32	114
	14	1.87 ± 0.14(3)	0.144	32	109
	18	4.01 ± 0.30(3)	0.148	30	99
	22	6.34 ± 0.46(3)	0.145	27	86
	26	9.32 ± 0.70(3)	0.144	24	78
	30	1.16 ± 0.21(4)	0.146	22	64
	34	1.22 ± 0.20(4)	0.145	18	65
	38	1.20 ± 0.25(4)	0.138	15	60

TABLE III. (*Continued*)

Element	E (MeV)	$\sigma_{Kx} \pm \delta\sigma_{Kx}$ [a] (b)	$K\beta/K\alpha$ [b]	$\Delta E_{K\alpha}$ [c] (eV)	$\Delta E_{K\beta}$ [c] (eV)
$_{23}$V	4	1.09 ± 0.09(1)	0.126	16	57
	6	4.87 ± 0.39(1)	0.120	21	90
	8	1.57 ± 0.12(2)	0.133	29	93
	10	3.91 ± 0.29(2)	0.160	33	118
	12	7.62 ± 0.55(2)	0.150	32	113
	14	1.27 ± 0.09(3)	0.157	30	114
	18	2.82 ± 0.20(3)	0.148	32	92
	22	4.77 ± 0.35(3)	0.140	27	84
	26	6.94 ± 0.51(3)	0.148	24	62
	30	9.08 ± 1.20(3)	0.142	23	68
	34	9.27 ± 0.71(3)	0.143	21	61
	38	1.12 ± 0.14(4)	0.135	19	56
$_{25}$Mn	4	4.00 ± 0.31	0.128	7	51
	6	1.89 ± 0.14(1)	0.133	15	66
	8	6.42 ± 0.48(1)	0.138	20	82
	10	1.47 ± 0.11(2)	0.142	23	97
	12	3.09 ± 0.22(2)	0.150	25	98
	14	5.67 ± 0.42(3)	0.160	28	101
	18	1.33 ± 0.10(3)	0.154	27	91
	22	2.35 ± 0.17(3)	0.153	26	85
	26	3.98 ± 0.29(3)	0.152	24	74
	30	5.40 ± 0.41(3)	0.148	21	75
	34	5.89 ± 0.64(3)	0.148	20	66
	38	6.49 ± 0.70(3)	0.143	18	59
$_{26}$Fe	4	3.51 ± 0.34	0.136	3	44
	6	1.62 ± 0.13(1)	0.131	10	69
	8	4.82 ± 0.36(1)	0.148	19	79
	10	1.08 ± 0.08(2)	0.160	24	96
	12	2.37 ± 0.17(2)	0.158	26	98
	14	4.13 ± 0.30(2)	0.159	24	100
	18	9.74 ± 0.70(2)	0.163	25	88
	22	1.80 ± 0.13(3)	0.161	23	79
	26	2.75 ± 0.20(3)	0.151	23	82
	30	4.03 ± 0.30(3)	0.150	21	81
	34	5.16 ± 0.40(3)	0.151	20	75
	38	5.77 ± 0.45(3)	0.148	18	68
$_{27}$Co	4	3.29 ± 0.33	0.132	5	25
	6	1.34 ± 0.10(1)	0.146	8	54
	8	3.70 ± 0.28(1)	0.155	17	79
	10	8.34 ± 0.62(1)	0.152	22	92
	12	1.68 ± 0.13(2)	0.154	24	94
	14	3.14 ± 0.23(2)	0.162	24	92
	18	7.51 ± 0.55(2)	0.162	26	90
	22	1.34 ± 0.10(3)	0.161	25	89
	26	2.21 ± 0.16(3)	0.157	24	73
	30	3.19 ± 0.24(3)	0.150	22	79
	34	4.53 ± 0.35(3)	0.157	22	77
	38	5.21 ± 0.40(3)	0.154	20	68

TABLE III. (*Continued*)

Element	E (MeV)	$\sigma_{Kx} \pm \delta\sigma_{Kx}$ [a] (b)	$K\beta/K\alpha$ [b]	$\Delta E_{K\alpha}$ [c] (eV)	$\Delta E_{K\beta}$ [c] (eV)
$_{28}$Ni	4	2.19 ± 0.19	0.152	2	35
	6	9.37 ± 0.70	0.140	7	50
	8	2.55 ± 0.19(1)	0.146	12	62
	10	5.85 ± 0.43(1)	0.149	19	81
	12	1.15 ± 0.08(2)	0.161	19	84
	14	2.09 ± 0.15(2)	0.162	22	85
	18	5.14 ± 0.37(2)	0.164	22	90
	22	9.49 ± 0.68(2)	0.164	25	89
	26	1.62 ± 0.12(3)	0.166	24	78
	30	2.35 ± 0.18(3)	0.158	20	71
	34	3.17 ± 0.24(3)	0.159	21	76
	38	4.01 ± 0.30(3)	0.155	19	67

[a] Numbers in parentheses denote powers of ten, e.g. 5.52 ± 1.10(3) = (5.52 ± 1.10) × 10^3. The absolute uncertainties in the cross sections are discussed in the text and in Table IV.

[b] The uncertainties in the $K\beta/K\alpha$ ratios are estimated to range between 6% and 9%.

[c] The uncertainties in the $K\alpha$ and $K\beta$ energy shifts are estimated to be <10 eV and <20 eV, respectively.

PWBA modified for binding-energy (B) and Coulomb-deflection (C) effects (PWBA-BC), the PWBA-BC modified for polarization (P) and relativistic (R) effects (PWBA-BCPR), and the PWBA-BCPR with electron-capture (EC) contributions. All theoretical ionization cross sections have been converted to the x-ray-production cross sections by means of the factor $\omega_0(\omega'/\omega)$, where ω_0 is the single-hole fluorescence yield and ω'/ω is the fluorescence-yield correction factor for multiple L-shell ionization given in Table V.

The BEA and PWBA direct-ionization theories are seen to overpredict the data by up to a factor of 10 for the higher-Z targets at the lower incident-ion energies. This has also been observed earlier for other incident-ion species.[22-28] Both the BEA and PWBA predictions do not exhibit the energy dependence of the experimental data. The PWBA with binding-energy and Coulomb-deflection modifications (PWBA-BC), both of which reduce the cross sections, is seen to be much lower than the PWBA, especially at lower incident-ion energies. The agreement between the PWBA-BC and the data at the lower incident-ion energies for the higher-Z elements is quite good. Most of the correction for binding energy and Coulomb deflection is due to the binding-energy effect. The modification for Coulomb deflection has been included in the calculations for completeness even though it is quite small in comparison to the binding energy effect as can be seen in Table II. The PWBA-BC modified for polarization and relativistic effects is seen to provide good predictions of the data for smaller Z_1/Z_2 values and to become progressively lower than the data as Z_1/Z_2 becomes larger. The polarization modification is found to be important primarily at higher ion velocities for larger Z_1/Z_2 ratios while the approximate correction for relativistic effects is more important at lower ion velocities for smaller Z_1/Z_2 ratios (see Table II).

For heavier incident ions, K-electron transfer to bound states of the projectile can be important to K-vacancy production in the target atom.[5-9] The contribution of electron capture (EC) depends strongly upon the incident-ion velocity and upon the ratio Z_1/Z_2. For solid targets, the EC contributions can be enhanced because of residual excitations of the incident-ion K-shell electrons due to multiple collisions in the solid.[64,65] The EC contributions presented in Fig. 3 have been determined by weighting the EC calculations of Lapicki and Losonsky[8] as modified by McDaniel *et al.*[9] for individual incident-charge states by the equilibrium charge-state fractions for $^{10}_{5}$B ions exiting from solids.[58,59] Equilibrium charge-state fractions of Marion and Young[58] were employed at 4 MeV. The equilibrium charge-state fractions of Wittkower and Betz[59] were employed at energies ≥ 12 MeV. Interpolated values of equilibrium charge-state fractions were used at 6, 8, and 10 MeV. This procedure assumes that charge-state equilibrium has been reached by the $^{10}_{5}$B ions in passing through the targets of thicknesses presented in Table I, and that these equilibrium distributions outside the solid are good representations of actual charge-state distributions in the solid. This seems to be a reasonable assumption, since at equilibrium for incident-ion energies

TABLE IV. Sources of uncertainty in the experimental x-ray-production cross sections.

Source	Range[a] (%)	Range[b] (%)
Counting statistics and background subtraction:		
$K\alpha$ and $K\beta$ x-ray yields	< 5	< 6
Rutherford-scattered $^{10}_{5}$B-ion yields	< 7	<10
Absolute efficiency:		
Source strength	< 3	
Source x-ray yields	< 4	
Calculation uncertainty		<11[c]
Particle-detector solid angle	< 3	< 3
Rutherford differential cross section through the uncertainty in the angle θ of the particle detector	< 4	< 4
Target-thickness effects[d]	< 5	<10
Total uncertainty (%)	<12[e]	<20[e]

[a] These ranges are valid for the data collected with the 0.10-mm Mylar installed.

[b] These ranges are valid for the data collected with the 0.013-mm Mylar installed.

[c] The uncertainty in the intrinsic efficiency calculation of the Si (Li) detector included a root-mean-square term of the uncertainties in the thicknesses and mass-absorption coefficients of the 0.013-mm Mylar attenuator, the Be window, the Au contact layer, and the Si dead layer.

[d] Multiple collisions in the solid target can produce residual excitation of the incident-ion K-shell electrons resulting in vacancy production in the target atom caused by electron capture. The additional uncertainty in the target x-ray production due to target-thickness effects has been estimated by considering the electron-capture contributions for the two extreme charge-state situations of the boron ion, i.e., the charge state of the boron ion is preserved or is equilibrated.

[e] The total uncertainty is the root mean square of the individual uncertainties.

above 14 MeV, 100% of the $^{10}_{5}$B ions have one or two K vacancies. At lower energies the percentage of $^{10}_{5}$B ions with one or two K vacancies decreases from 95% at 14 MeV to 50% at 4 MeV. The contributions of electron capture have been added to the direct-ionization calculations for the fully modified PWBA in Fig. 3 and is found to provide good agreement with the data. Theoretical estimates indicate that the EC contributions, which represent 25% of the total ionization for $_{15}$P and 6% of the total ionization for $_{28}$Ni at the highest energies, increase with increasing Z_1/Z_2.

The importance of direct ionization for the present Z_1/Z_2 ratios at these energies can be seen more easily in the form of a universal plot. In the PWBA formalism the measured cross sections should exhibit a universal behavior for all values of the variables η_K and θ_K when scaled by the Coulomb-deflection modification $[9E_{10}(b\zeta\theta_K\eta_K^{-3/2})]$, the relativistic correction (R), and the appropriate fluorescence yield $(\omega_0\omega'/\omega)$ and $(\sigma_{0K}/\zeta\theta_K)$.

Figure 4 presents the data in terms of an experimentally inferred F^{expt} given by

$$F\left(\frac{\eta_K}{\zeta^2\theta_K^2}\right)^{\text{expt}} = \frac{\sigma_{Kx}^{\text{expt}} - \sigma_C(\omega_0\omega'/\omega)}{R(\omega_0\omega'/\omega)9E_{10}(b\zeta\theta_K\eta_K^{-3/2})(\sigma_{0K}/\zeta\theta_K)}\ , \tag{9}$$

where σ_C is the cross section for electron capture. The electron-capture contribution to ionization has been subtracted from the measurements. The solid line in Fig. 4 is the theoretical direct-ionization universal function, $F(\eta_K/\zeta^2\theta_K^2)$, which does not include contributions from electron capture. The experimental data fall on or near the curve which represents the direct-ionization theory.

VI. CONCLUSIONS

The present work makes comparisons between experimental x-ray-production cross sections and theory for ranges of the parameters Z_1/Z_2 and v_1/v_e, where Coulomb ionization should be the

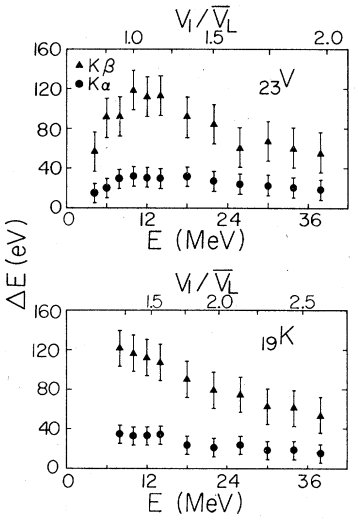

FIG. 2. X-ray-energy shifts of K_α and K_β transitions for $^{10}_{5}$B-ion bombardment of $_{19}$K and $_{23}$V. The maximum x-ray-energy shift is observed when the ratio of ion velocity (v_1) to the average L-shell-electron velocity $(\bar{v}_L)$ is close to one, indicating that the majority of the K x-ray-energy shifts are due to multiple L-shell vacancies that are present at the time of the K-vacancy decay. $v_1/\bar{v}_L = (E_1/\lambda\bar{U}_L)^{1/2}$, where E_1 is the incident $^{10}_{5}$B-ion energy, λ is the ratio of $^{10}_{5}$B-ion mass to electron mass, and $\bar{U}_L = \frac{1}{4}(U_{L1} + U_{L2} + 2U_{L3})$ is the average L-shell-electron binding energy.

TABLE V. Ratios of the fluorescence yield calculated for multiple $2p$ vacancies to the fluorescence yield calculated for the *no-defect* configuration by the procedure for Larkins (Ref. 61). Numerical values of the fluorescence yield for single-hole ionization are taken from the fitted values of Bambynek *et al.* (Ref. 60).

E (MeV) \ ω_0	$_{15}$P 0.060	$_{19}$K 0.138	$_{20}$Ca 0.163	$_{21}$Sc 0.190	$_{22}$Ti 0.219	$_{23}$V 0.250	$_{25}$Mn 0.313	$_{26}$Fe 0.347	$_{27}$Co 0.381	$_{28}$Ni 0.414
4			1.14	1.10	1.08	1.06	1.03	1.02	1.01	1.01
6			1.16	1.12	1.11	1.08	1.05	1.04	1.03	1.02
8	1.17	1.22	1.18	1.13	1.12	1.10	1.06	1.05	1.04	1.03
10	1.17	1.21	1.18	1.15	1.13	1.12	1.07	1.07	1.06	1.04
12	1.18	1.21	1.18	1.15	1.13	1.12	1.07	1.07	1.06	1.04
14		1.20	1.17	1.14	1.13	1.11	1.08	1.07	1.06	1.05
18		1.15	1.15	1.13	1.12	1.11	1.08	1.06	1.06	1.05
22	1.10	1.14	1.13	1.11	1.10	1.09	1.07	1.06	1.06	1.05
26	1.10	1.14	1.13	1.09	1.09	1.08	1.06	1.06	1.05	1.04
30	1.09	1.11	1.11	1.09	1.08	1.08	1.06	1.06	1.05	1.04
34	1.09	1.11	1.10	1.09	1.08	1.07	1.05	1.05	1.05	1.04
38	1.08	1.09	1.09	1.08	1.07	1.06	1.05	1.05	1.04	1.04

primary excitation mechanism. The direct-ionization theories, modified for increased target-electron binding, Coulomb deflection of the incident ion, polarization of the target-electron wave functions, and relativistic target-electron velocities are found to provide very good representations of the data for $Z_1/Z_2 \lesssim 0.25$.

The theoretical calculations of direct Coulomb ionization indicate the following general features. The binding-energy effect is the dominant modifi-

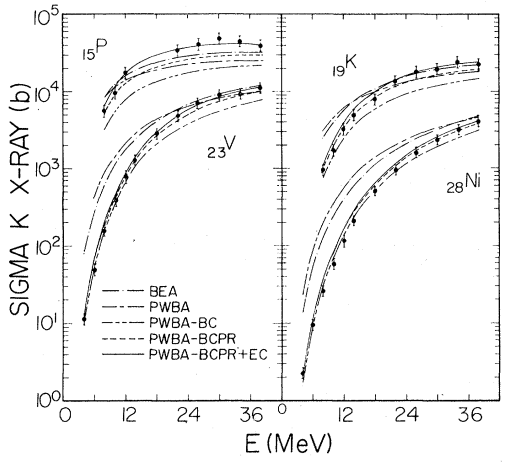

FIG. 3. K-shell x-ray-production cross sections for $^{10}_{5}$B-ion bombardment of thin solid targets of $_{15}$P, $_{19}$K, $_{23}$V, and $_{28}$Ni. The experimental data are compared to the direct-ionization predictions of the BEA, the PWBA, the PWBA modified for binding-energy (B) and Coulomb-deflection (C) effects (PWBA-BC), and the PWBA-BC modified for polarization (P) and relativistic (R) effects (PWBA-BCPR). Electron-capture (EC) contributions have been added to the fully modified PWBA. All theoretical ionization cross sections have been converted to x-ray-production cross sections by the fluorescence yield for single-hole ionization (ω_0) and by the fluorescence-yield correction factor for multiple ionization (ω'/ω) as given in Table V.

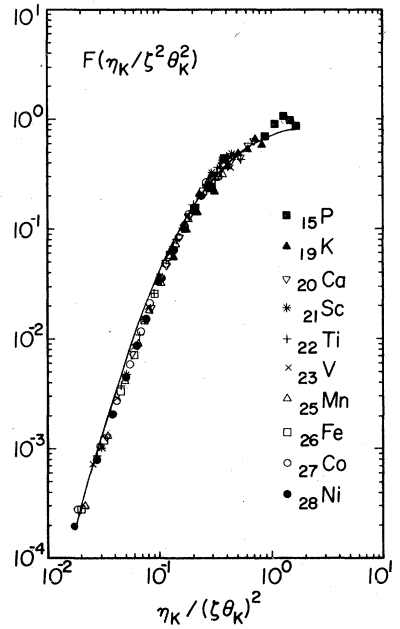

FIG. 4. Experimental x-ray-production cross sections for $^{10}_{5}$B-ion bombardment scaled as a function of $\eta_K/\zeta^2\theta_K^2$ for comparison to the approximate universal function $F(\eta_K/\zeta^2\theta_K^2)$ in the PWBA theory of Basbas *et al.* (Refs. 18–21). The experimentally inferred function $F(\eta_K/\zeta^2\theta_K^2)^{\text{expt}}$ is given in the text and includes changes in the fluorescence yields due to multiple ionization as given in Table V. The theoretical universal function is given by the solid line.

cation especially at lower incident-ion velocities producing a decrease in the cross section by a factor ≤ 10. Coulomb-deflection effects are small for these "heavy" $^{10}_{5}$B ions and produce a decrease in the cross sections of $\leq 15\%$. Polarization is important at higher velocities for larger values of Z_1/Z_2. For the largest Z_1/Z_2 ratio of the present work, the maximum increase in the cross section was 27%. The approximate correction for relativistic effects is small except at lower incident-ion velocities for the larger-Z elements. For 4-MeV $^{10}_{5}$B ions incident on $_{28}$Ni, the relativistic correction increased the cross section by ~20%.

Electron capture is believed to be an important consideration for the larger ratios of Z_1/Z_2 and at higher incident-ion velocities. For 38-MeV $^{10}_{5}$B ions incident on $_{15}$P, the theoretical estimates of direct-ionization and electron-capture contributions to vacancy production in $_{15}$P was ~75% and ~25%, respectively. We note a need for a consistent set of equilibrium-charge-state fractions which span a large range of incident velocities for heavy ions incident on solid targets.

Changes in fluorescence yields caused by the effects of multiple ionization were found to be most important at incident-ion velocities which match target L-shell-electron velocities and for larger values of Z_1/Z_2.

ACKNOWLEDGMENTS

The authors wish to acknowledge J. Lin, R. P. Chaturvedi, R. M. Wheeler, S. J. Cipolla, K. A. Kuenhold, L. A. Rayburn, D. E. Johnson, and W. O. Holland for their assistance with the data acquisition. We would like to thank G. Lapicki for providing the electron-capture calculations prior to publication and George Basbas for helpful discussions. The experiments were performed on the Tandem Van de Graaff Accelerator at Oak Ridge National Laboratory, which is supported by the Energy Research and Development Administration and operated by the Union Carbide Corporation. Travel to ORNL was provided by Oak Ridge Associated Universities. The North Texas State University Research was supported in part by the North Texas State University Organized Research Funds, the Robert A. Welch Foundation. and the Research Corporation. Acknowledgment is made to the donors of the Petroleum Research Fund administered by the American Chemical Society for partial support of this research.

---

*Present address: Directorate of Combat Development, United States Army Field Artillery School, Ft. Sill, Okla. 73503.

[1]See, for example, D. H. Madison, and E. Merzbacher, *Atomic Inner-Shell Processes*, edited by Bernd Crasemann (Academic, New York, 1975), Vol. 1, p. 1.

[2]U. Fano and W. Lichten, Phys. Rev. Lett. 14, 627 (1965).

[3]M. Barat and W. Lichten, Phys. Rev. A 6, 211 (1972).

[4]See, for example, Fig. 13 of Ref. 1.

[5]J. R. Macdonald, L. M. Winters, M. D. Brown, T. Chiao, and L. D. Ellsworth, Phys. Rev. Lett. 29, 1291 (1972); J. R. Macdonald, L. M. Winters, M. D. Brown, L. D. Ellsworth, T. Chiao, and E. W. Pettus, *ibid.* 30, 251 (1973); J. R. Macdonald, P. Richard, C. L. Cocke, M. Brown, and I. A. Sellin, *ibid.* 31, 684 (1973); L. M. Winters, J. R. Macdonald, M. D. Brown, T. Chiao, L. D. Ellsworth, and E. W. Pettus, Phys. Rev. A 8, 1835 (1973).

[6]J. R. Mowat, I. A. Sellin, P. M. Griffin, D. J. Pegg, and R. S. Peterson, Phys. Rev. A 9, 644 (1974).

[7]F. Hopkins, Phys. Rev. Lett. 35, 270 (1975); F. Hopkins, N. Cue, and V. Dutkiewicz, Phys. Rev. A 12, 1710 (1975); F. Hopkins, R. Brenn, A. R. Whittemore, N. Cue, and R. P. Chaturvedi, Phys. Lett. A 53, 79 (1975); F. Hopkins, R. Brenn, A. R. Whittemore, N. Cue, V. Dutkiewicz, and R. P. Chaturvedi, Phys. Rev. A 13, 75 (1976).

[8]G. Lapicki and W. Losonsky, Phys. Rev. A 15, 896 (1977).

[9]F. D. McDaniel, J. L. Duggan, G. Basbas, P. D. Miller, and G. Lapicki, Phys. Rev. A 16, 1375 (1977).

[10]N. Cue, V. Dutkiewicz, P. Sen, and H. Bakhru, Phys. Rev. Lett. 32, 1155 (1974).

[11]J. D. Garcia, E. Gerjuoy, and J. W. Welker, Phys. Rev. 165, 66 (1968); J. D. Garcia, Phys. Rev. A 1, 1402 (1970); 1, 280 (1970).

[12]J. Bang and J. M. Hansteen, K. Dan. Vidensk. Selsk. Mat.-Fys. Medd. 31, No. 13 (1959).

[13]J. M. Hansteen and O. P. Mosebekk, Z. Phys. 234, 281 (1970); Nucl. Phys. A 201, 541 (1973).

[14]E. Merzbacher and H. Lewis, *Encyclopedia of Physics*, edited by S. Flügge (Springer-Verlag, Berlin, 1958), Vol. 34, p. 166.

[15]G. S. Khandelwal and E. Merzbacher, Phys. Rev. 144, 349 (1966); 151, 12 (1966).

[16]B. K. Thomas and J. D. Garcia, Phys. Rev. 179, 94 (1969).

[17]J. S. Hansen, Phys. Rev. A 8, 822 (1973).

[18]G. Basbas, W. Brandt, and R. Laubert, Phys. Rev. A 7, 983 (1973).

[19]G. Basbas, W. Brandt, R. Laubert, and A. Schwarzschild, Phys. Rev. Lett. 27, 171 (1971).

[20]G. Basbas, W. Brandt, and R. Laubert, Phys. Lett. A 34, 277 (1971).

[21]G. Basbas, W. Brandt, and R. Laubert, Phys. Rev. A 17, 1655 (1978).

[22]F. D. McDaniel, T. J. Gray, and R. K. Gardner, Phys. Rev. A 11, 1607 (1975).

[23]F. D. McDaniel, T. J. Gray, R. K. Gardner, G.M.

Light, J. L. Duggan, H. A. Van Rinsvelt, R. D. Lear, G. H. Pepper, J. W. Nelson, and A. R. Zander, Phys. Rev. A 12, 1271 (1975).
[24]T. J. Gray, P. Richard, R. L. Kauffman, T. C. Holloway, R. K. Gardner, G. M. Light, and J. Guertin, Phys. Rev. A 13, 1344 (1976).
[25]G. Bissinger, P. H. Nettles, S. M. Shafroth, and A. L. Waltner, Phys. Rev. A 10, 1932 (1974).
[26]F. D. McDaniel, J. L. Duggan, P. D. Miller, and G. D. Alton, Phys. Rev. A 15, 846 (1977).
[27]J. Tricomi, J. L. Duggan, F. D. McDaniel, P. D. Miller, R. P. Chaturvedi, R. M. Wheeler, J. Lin, K. A. Kuenhold, L. A. Rayburn, and S. J. Cipolla, Phys. Rev. A 15, 2269 (1977).
[28]S. R. Wilson, F. D. McDaniel, J. R. Rowe, and J. L. Duggan, Phys. Rev. A 16, 903 (1977).
[29]W. E. Meyerhof, Phys. Rev. Lett. 31, 1341 (1973).
[30]W. E. Meyerhof, Phys. Rev. A 10, 1005 (1974).
[31]W. E. Meyerhof, R. Anholt, T. K. Saylor, and P. D. Bond, Phys. Rev. A 11, 1083 (1975).
[32]W. E. Meyerhof and R. Anholt, *Proceedings of the Fourth International Conference on Scientific and Industrial Applications of Small Accelerators, Denton, Texas, 1976,* edited by J. L. Duggan and I. L. Morgan, (IEEE, New York, 1976), p. 60.
[33]W. E. Meyerhof, R. Anhold, T. K. Saylor, S. M. Lazarus, A. Little, and L. F. Chase, Jr., Phys. Rev. A 14, 1653 (1976).
[34]W. E. Meyerhof, R. Anholt, and T. K. Saylor, Phys. Rev. A 16, 169 (1977).
[35]R. Anholt and W. E. Meyerhof, Phys. Rev. A 16, 190 (1977).
[36]W. E. Meyerhof, *Abstracts of the Fifth International Conference on Atomic Physics, Berkeley, California, July 1976,* edited by R. Marrus, M. H. Prior, and H. A. Shagart (University of California, Berkeley, 1976); W. E. Meyerhof, R. Anholt, J. Eichler, and A. Salop (unpublished).
[37]B. Fastrup, in *The Physics of Electronic and Atomic Collisions,* edited by J. S. Risley and R. Geballe (University of Washington, Seattle, 1975), p. 361.
[38]G. Monigold, F. D. McDaniel, J. L. Duggan, R. Mehta, R. Rice, and P. D. Miller, *Proceedings of the Fourth International Conference on Scientific and Industrial Applications of Small Accelerators, Denton, Texas, 1976,* edited by J. L. Duggan and I. L. Morgan (IEEE, New York, 1976), p. 70.
[39]L. B. Magnusson, Phys. Rev. 107, 161 (1957); R. J. Gehrke and R. A. Lokken, Nucl. Instrum. Methods 97, 219 (1971); J. S. Hansen, J. C. McGeorge, D. Nix, W. D. Schmidt-Ott, I. Unus, and R. W. Fink, *ibid.* 106, 365 (1973); J. L. Campbell and L. A. McNelles, *ibid.* 117, 519 (1974); 125, 205 (1975).
[40]W. J. Gallagher and S. J. Cipolla, Nucl. Instrum. Methods 122, 405 (1974).
[41]J. J. Simpson, J. A. Cookson, D. Ecclesmall, and M. O. L. Yates, Nucl. Phys. 62, 385 (1965).
[42]A W. Obst, D. L. McShan, and R. H. Davis, Phys. Rev. C 6, 1814 (1972).
[43]R. Laubert, H. Haselton, J. R. Mowat, R. S. Peterson, and I. A. Sellin, Phys. Rev. A 11, 135 (1975).
[44]E. M. Berstein and H. W. Lewis, Phys. Rev. 95, 83 (1954); C. W. Lewis, R. L. Watson, and J. B Natowitz, Phys. Rev. A 5, 1773 (1972); L. M. Middleman, R. L. Ford, and R. Hofstadter, *ibid.* 2, 1429 (1970); E. H. Pedersen, S. J. Czuchlewski, M. D. Brown, L. D. Ellsworth, and J. R. Macdonald, *ibid.* 11, 1267 (1975).
[45]K. Taulbjerg and P. Sigmund, Phys. Rev. A 5, 1285 (1976).
[46]K. Taulbjerg, B. Fastrup, and E. Laegsgaard, Phys. Rev. A 8, 1814 (1973).
[47]W. Brandt and R. Laubert, Phys. Lett. A 43, 53 (1973).
[48]D. Burch and K. Taulbjerg, Phys. Rev. A 12, 508 (1975).
[49]J. T. Routti and S. G. Prussin, Nucl. Instrum Methods 72, 125 (1969).
[50]J. H. McGuire and P. Richard, Phys. Rev. A 8, 1374 (1973).
[51]G. S. Khandelwal, B. H. Choi, and E. Merzbacher, At. Data 1, 103 (1969).
[52]R. Rice, G. Basbas, and F. D. McDaniel, At. Data Nucl. Data Tables 20, 503 (1977).
[53]D. Jamnik and C. Zupancic, K. Dan. Vidensk. Selsk. Mat.-Fys. Medd. 31, No. 2 (1957).
[54]B. H. Choi, Phys. Rev. A 4, 1002 (1971).
[55]V. S. Nikolaev, Zh. Eksp. Teor. Fiz. 51, 1263 (1966) [Sov. Phys. JETP 24, 847 (1967)].
[56]J. R. Oppenheimer, Phys. Rev. 31, 349 (1928).
[57]H. C. Brinkman and H. A. Kramers, Proc. Acad. Sci. (Amsterdam) 33, 973 (1930).
[58]J. B. Marion and F. C. Young, *Nuclear Reaction Analysis* (North-Holland, Amsterdam, 1968), p. 34.
[59]A. B. Wittkower and H. D. Betz, At. Data 5, 113 (1973).
[60]W. Bambynek, B. Craseman, R. W. Fink, H. U. Freund, H. Mark, C. D. Swift, R. E. Price, and P. V. Rao, Rev. Mod. Phys. 44, 716 (1972).
[61]F. P. Larkins, J. Phys. B 4, L29 (1971).
[62]E. J. McGuire, Phys. Rev. A 2, 273 (1970).
[63]F. Herman and S. Skillman, *Atomic Structure Calculations* (Prentice-Hall, Englewood Cliffs, N.J., 1963)
[64]F. Hopkins, Phys. Rev. Lett. 35, 270 (1975).
[65]T. J. Gray, P. Richard, K. A. Jamison, J. M. Hall, and R. K. Gardner, Phys. Rev. A 14, 1333 (1976).